Computers and Electronics in Agriculture 246 (2026) 111587

Contents lists available at ScienceDirect

Computers and Electronics in Agriculture

journal homepage: www.elsevier.com/locate/compag

Original papers

Air-assisted sprayer airflow interaction with traditional olive orchard canopies and its effect on spray distribution

Alba Vigo-Morancho [a,*], María Videgain [a,b], Alfredo Serreta [a], Antonio Boné [a], Mariano Vidal [a], Francisco Javier García-Ramos [a,b]

[a] Escuela Politécnica Superior, Universidad de Zaragoza, Ctra. Cuarte s/n, 22071 Huesca, Spain
[b] Instituto Agroalimentario de Aragón—IA2 (CITA-Universidad de Zaragoza), EPS, Universidad de Zaragoza, Carretera de Cuarte s/n, E- 22071 Huesca, Spain

ARTICLE INFO

Keywords:
Air velocity
Coverage
LiDAR
Pesticide
Fan

ABSTRACT

Air-assisted sprayers currently incorporate mechanisms that allow modification of airflow outlet characteristics, which is a key factor in product distribution quality. However, limited information exists on how airflow interacts with complex tree canopies, particularly in traditional olive orchards. The aim of this study was to model the behavior of airflow velocity generated by a previously laboratory characterized air assisted sprayer in a traditional olive orchard, as a function of air flow configuration (fan gearbox) and operational and canopy structural parameters.

Five olive trees were selected, and a three-dimensional grid of 64 measurement points (4 depths × 4 sections × 4 heights) was defined, where airflow velocity (m s^{-1}) was recorded with a vane probe anemometer under two sprayer configurations. Canopy characterization was carried out using Light Detection and Ranging (LiDAR) measurements, from which both canopy volume (m^3) and density based on the number of impacts (NI) at each sampling location were determined. In addition, manual defoliations of 0.008 m^3 cubes were performed at 8 positions per canopy, allowing a correlation between impacts and leaf area density (LAD, m^2 m^{-3}) to be established ($R^2 = 0.61$).

Airflow within the canopy was characterized, and a model including sprayer gear setting, measurement depth, height, and categorized vegetation density (low or high density, LD or HD, respectively, based on the accumulated number of impacts across trees, NIa) explained 72% of the observed variability in air velocity inside the tree canopy. Spray performance was evaluated at the same sampling points using water-sensitive papers (WSP) and tracer collectors (manganese, Mn), allowing the effects of application parameters on coverage (%) and deposition (μg cm^{-2}) to be quantified. These effects were largely consistent with those influencing air velocity, which was strongly correlated with both coverage and deposition. Notably, adequate coverage and deposition levels were predominantly associated with air velocities inside the canopy exceeding 2 m s^{-1}, providing valuable insight for optimizing sprayer adjustment and operating conditions.

1. Introduction

Efficient application of plant protection products in three-dimensional (3D) crops largely depends on the performance of air-assisted sprayers. These systems were introduced to the market several decades ago to overcome the limitations of conventional hydraulic systems, which tend to concentrate the spray on the canopy periphery, resulting in poor internal coverage and low deposition uniformity (Cross et al., 2003). The pneumatic system, generally based on an axial or radial fan that generates an airstream discharged through diffusers, has several functions, such as moving the vegetation to improve spray penetration into inner zones, and transporting the sprayed droplets towards the target. However, improper adjustment of the airflow can lead to adverse effects, causing product losses either by drift under excessive airflow, or by runoff under insufficient airflow (Fox et al., 2008; Garcera et al., 2017; Salas et al., 2022; Salcedo et al., 2021).

The influence of application parameters on airflow behavior generated by these sprayers was initially studied in pioneering works such as those of Reichard et al. (1979), Fox et al. (1992), or Svensson (2001), who characterized air velocity patterns produced by different designs of

* Corresponding author.
E-mail address: albavm@unizar.es (A. Vigo-Morancho).

https://doi.org/10.1016/j.compag.2026.111587
Received 29 October 2025; Received in revised form 22 January 2026; Accepted 18 February 2026

air assisted sprayers. These designs have evolved considerably over time, and research efforts have evolved accordingly. At present, many sprayer models incorporate mechanisms that allow modifications of the airflow conditions through, for example, variable-section diffusers, fans with multi-speed gearboxes, or even systems for independent air regulation on each side of the machine. These advances aim to improve spray efficiency and minimize drift. However, the mere availability of adjustment mechanisms does not guarantee precise application. To take advantage of these mechanisms, it is necessary to have a detailed knowledge of airflow characteristics in the vicinity of the sprayer and, in addition, to understand how this airflow changes when interacting with the crop. This aspect has been addressed in high-impact projects such as the ISAFRUIT project, in which airflow behavior was studied under section restrictions and where an in-line regulation device was implemented, enabling independent and automatic airflow adjustment on the left and right sprayer sections depending on wind conditions and sprayer position relative to the presence or absence of crop rows (Doruchowski et al., 2009). In the same line, and more recently, these authors developed a sprayer with two towers and independent hydraulic fans (left/right), which operated in asymmetric conditions, reducing ground losses by 25% and drift by 50% compared with symmetric operation (Doruchowski et al., 2023).

Other authors have characterized this type of equipment through direct measurements using hot-wire, vane, or ultrasonic anemometers (García-Ramos et al., 2012; Salcedo et al., 2019; Sozzi, 2011; Vigo-Morancho et al., 2024), or through CFD (Computational Fluid Dynamics) simulations (Badules et al., 2018; Endalew et al., 2010; Zhang et al., 2024). These studies have led to the development of predictive models of air velocity module as a function of fan operating conditions and nozzle system geometry, providing information on airflow characteristics at the crop perimeter. Once air penetrates the canopy, its velocity is reduced by canopy resistance, which depends on structural variables such as canopy volume or the spatial density of leaves and branches. Some authors have studied the optimal airflow configuration according to crop type, for example, Garcera et al. (2022) tested multiple configurations in three air assisted sprayers with the aim of integrating results into a decision support tool and showed the importance of reducing fan gear ratio and selecting appropriate nozzles to better match spray patterns to canopy geometry. Similarly, Salas et al. (2022) characterized airflow in a sprayer equipped with real-time variable rate dosing technology, later applying these results in field validation tests (Salas et al., 2025). In this case, airflow was measured using a three-dimensional anemometer at the front and rear of an artificial canopy that had been previously characterized. Grella et al. (2022a) related the optimal fan airflow with Leaf Area Index (LAI) in vineyards and demonstrated that excessive airflow reduced deposition, proposing variable airflow settings as an experimental guideline to be incorporated at a later stage into the control algorithm of a prototype sprayer capable of continuously adjusting fan speed (Grella et al., 2022b). Similarly, Jeon and Zhu (2024) characterized airflow at the sprayer outlet and at 1 m distance in a machine equipped with PWM (Pulse Width Modulation) controllers to regulate fan speed, obtaining decay profiles around the sprayer and correlating them with deposition results across different LAI ranges for each configuration. In this way, they proposed a multivariable model to predict the required PWM value as a function of LAI.

Along these lines, a complementary approach is to characterize airflow evolution within the crop, integrating measurements within the canopy that allow modelling air velocity as a function of canopy architecture and sprayer settings. A practical example of this approach is provided by Feng et al. (2024), who measured airflow both at the outlet and inside apple tree canopies, together with deposition and drift, and implemented graded airflow control through an adjustable inlet mechanism according to canopy structure.

Canopy characterization is another fundamental aspect to be considered when addressing variable rate input applications. A precise understanding of canopy geometry and density is essential to assess their influence on key adjustable parameters, including application dose or, in this case, sprayer airflow. Currently, several studies are focused on finding technologies that can determine these parameters accurately and non-destructively. LiDAR (Light Detection and Ranging) scanners are among the most widely used and studied options (Li et al., 2017; Torrent et al., 2025; Zhou et al., 2021). This technology emits laser pulses and measures the return time of reflected signals, generating high precision point clouds that reconstruct canopy structure and foliage distribution (Pagliai et al., 2022; Petrović et al., 2022). As an example, in the aforementioned study of Feng et al. (2024), canopy structure was characterized using a model previously defined by Gu et al. (2022), in which leaf area was modelled from LiDAR point density.

It should be noted that this technology is costly, which has encouraged the search for alternative methods that, once validated against accurate LiDAR results, can provide canopy traits at a lower cost. One such example is the work of Miranda-Fuentes et al. (2015), who evaluated several methods for estimating the volume of traditionally trained olive trees, obtaining good correlations by calculating the mean vector of vertical canopy projection.

Most of the above-mentioned studies on airflow adjustment in air assisted sprayers have been carried out in vineyards, citrus orchards, and apple trees. In Spain, olive cultivation covers about 2.8 million hectares, representing almost 17% of the total crop area. Furthermore, 45% of plantations have densities below 140 trees per hectare (MAPA, 2024a), typical of traditional olive orchards. Consequently, machinery acquisition for this sector is significant, in 2024, more than 3,000 new air assisted sprayers were registered in the Official Register of Agricultural Machinery (ROMA) (MAPA, 2024).

Despite the significant progress achieved in variable-rate pesticide application, the lack of quantitative knowledge about how airflow attenuates inside complex tree canopies remains a major limitation for current smart spraying systems. Most variable-rate technologies have focused on adjusting liquid flow rate, while airflow configurations are still commonly defined as fixed or only indirectly regulated. Although previous researches have explored variable air- assistance systems and airflow adjustment concepts (Hołownicki et al., 2017; Grella et al., 2022a), robust and transferable criteria to relate canopy structure with in-canopy airflow behavior are still missing. In particular, the absence of explicit relationships linking measurable canopy structural descriptors to in-canopy airflow attenuation hinders the integration of airflow regulation into smart spraying decision-making frameworks.

Within this context, the national PIVOS project ("*Smart spraying for a sustainable vineyards and olive trees*", PID2019-104289RB, https://pivos.upc.edu/), and its continuation through the ADOPTA project (PDC2022-133395), both funded by the Spanish Ministry of Science and Innovation, have addressed the development and field validation of intelligent air-assisted sprayers following two complementary research lines. On the one hand, these projects have focused on the development and validation of variable-rate liquid application systems based on sensors, prescription maps, and PWM-based flow control, which have already been successfully tested under field conditions (Biscamps et al., 2025; Ortí et al., 2022; Rovira-Más et al., 2024). On the other hand, they have also encompassed experimental studies aimed at improving the understanding of airflow behavior and its interaction with canopy structure as a necessary step toward airflow adjustment. Within this framework, the present study proposes a practical methodological approach for airflow adjustment in air-assisted sprayers adapted to traditional olive orchards, integrating the sprayer's wind map (air velocity at the canopy boundary) and the canopy structural characterization based on LiDAR data. Specifically, the objectives of this work were to (1) develop and describe a methodology to characterize canopy structure and density using terrestrial LiDAR data, introducing the accumulated number of impacts (NIa) as a structural descriptor to account for vegetation influence on in-canopy airflow; (2) develop and validate a predictive model describing airflow velocity decay inside the canopy as a function of sprayer settings and canopy structure; and (3) quantify the effect of airflow

configuration on spray coverage and deposition in traditional olive orchards, in order to demonstrate the relevance of the proposed methodology for supporting airflow regulation strategies in intelligent spraying systems.

The final aim is to provide a consistent basis for defining airflow regulation strategies in variable-rate air-assisted sprayers, supporting future research and the practical calibration of smart spraying systems.

2. Material and methods

2.1. Sprayer features and experimental site

The experimental work was carried out using the Twister S6 commercial air-blast sprayer for traditional olive orchards (Mañez y Lozano S.L., Valencia, Spain) (Fig. 1), which was previously modified within the framework of the PIVOS project to operate as an intelligent spraying platform. This sprayer configuration and its liquid application control system have been described and preliminarily evaluated under laboratory conditions in previous studies (Ortí et al., 2022). This sprayer has a main tank with a capacity of 1,500 L and an air assist system with a conventional axial fan generating an air jet discharged through a curved nozzle arc, targeting both sides of the canopy. The liquid application system incorporates 16 pulse-width-modulated (PWM) solenoid valves installed at nozzles (115880 e-ChemSaver, TeeJet Technologies, Glendale Heights, IL, USA), allowing sector-based regulation of the spray flow rate without modifying the system pressure. The nozzles are electronically actuated at a fixed frequency (10 Hz), with the duty cycle determining the effective flow rate delivered by each nozzle.

The control architecture is based on an onboard industrial computer connected to a data acquisition system, which records key operational parameters such as system pressure and total flow rate through dedicated sensors installed in the main hydraulic circuit. The sprayer can operate under two working modes: 1) a manual mode, enabling independent activation and configuration of predefined nozzle sectors for experimental purposes, and 2) an automatic mode, designed to apply prescription maps for variable-rate liquid application based on georeferenced information (Ortí et al., 2022).

In this case, for the purposes of the present study, a 100% duty cycle was used; that is, the valves remained fully open during the entire 100 ms activation interval. The experimental plot was located in the municipality of Lupiñén (Huesca; 42° 10′ 58.5″ N 0° 34′ 21.8″ W) and consisted of a traditional olive orchard (*Olea europaea* L., cv. Picual) with a 7 × 7 m planting frame.

Fig. 1. Twist S6 air assisted sprayer (Mañez Lozano, Spain) used in the experiments.

2.2. Sampling points and canopy characterization

Five experimental trees were selected, based on structural and density criteria, to conduct the airflow and spray deposition tests, which were all performed on the half of the canopy exposed to the sprayer in a single row pass.

Inside the canopy of each tree, a fixed grid of sampling points was established for airflow and deposition measurements. Specifically, a total of 64 points were defined from the intersections of four measurement planes in height, four planes in the transverse section, and four planes in the longitudinal section (Fig. 2). For this purpose, 16 wooden stakes were arranged in a 50 × 70 cm frame at the base of each tree (Fig. 2a), forming a rectangular measurement grid with the trunk centered on the innermost measurement plane (D4). At each stake position, a vertical mast 3.5 m in height was installed. Along each mast, four fixed measurement levels were defined at 170, 220, 270, and 320 cm above ground surface, resulting in the three-dimensional grid of 64 sampling points shown in Fig. 2b.

2.2.1. LiDAR canopy characterization

Canopy characterization of each tree was carried out using an RTC360 terrestrial laser scanner (Leica Geosystems, Heerbrugg, Switzerland), a high-precision device designed for rapid and detailed environmental scanning based on LiDAR technology. This equipment provides an acquisition rate of up to 2 million points per second and a scanning range from 0.5 to 130 m. For each tree, data acquisition was carried out from eight scanning stations following a multi-scan strategy aimed at ensuring a complete, homogeneous three-dimensional reconstruction of the canopy while minimizing occlusion effects. Four scanning stations were positioned around each tree at the vertices of a 7 × 7 m square, corresponding to the planting frame, with the trunk axis located at the center. At these peripheral locations, the scanner was mounted at a height of 1.40 m above ground level, allowing uniform external coverage of the canopy (Fig. 3a). An additional four scanning stations were placed beneath the canopy projection (Fig. 3b) to improve the capture of internal canopy structure and volumetric density. Three of these under-canopy positions were distributed along the stakes defining the fixed grid used for airflow velocity and spray coverage measurements, within the evaluated half of the canopy, while a fourth station was located beneath the center of the non-evaluated half.

The individual scans were automatically registered by the scanner software to generate a unified three-dimensional point cloud for each tree. This automatic registration is performed by the scanner software, which aligns multiple scan positions into a single, internally consistent point cloud using a Simultaneous Localization and Mapping (SLAM) approach, without the need for external targets or absolute georeferencing (Biasion et al., 2019).

The resulting point clouds were extracted in Cartesian coordinates (X, Y, Z) and imported into CloudCompare® (TelecomParisTech, Paris, France) for data management. Each point cloud was reoriented so that the X-axis corresponded to the row direction (length), the Y-axis to olive canopy width, and the Z-axis to olive canopy height. Points corresponding to the ground, surroundings, and stakes were removed, as well as the portion of the trunk below the canopy.

Canopy volume (V, m^3) was calculated following a procedure similar to that described by Xu et al. (2013) and Miranda-Fuentes et al. (2015). Canopy point cloud was divided into horizontal slices. The points of each slice were then projected onto the same horizontal plane and a closed polyline was generated to this projection to accurately define the contour of the section. The internal area of this polyline was calculated using AutoCAD software (Autodesk, Inc., San Rafael, CA, USA) and the partial volume of each slice was obtained by multiplying the corresponding area by the slice height, established at 0.05 m to facilitate the processing of the numerous extracted layers given the large tree volume. Finally, canopy volume was obtained by numerically integrating the areas of all slices across the canopy height.

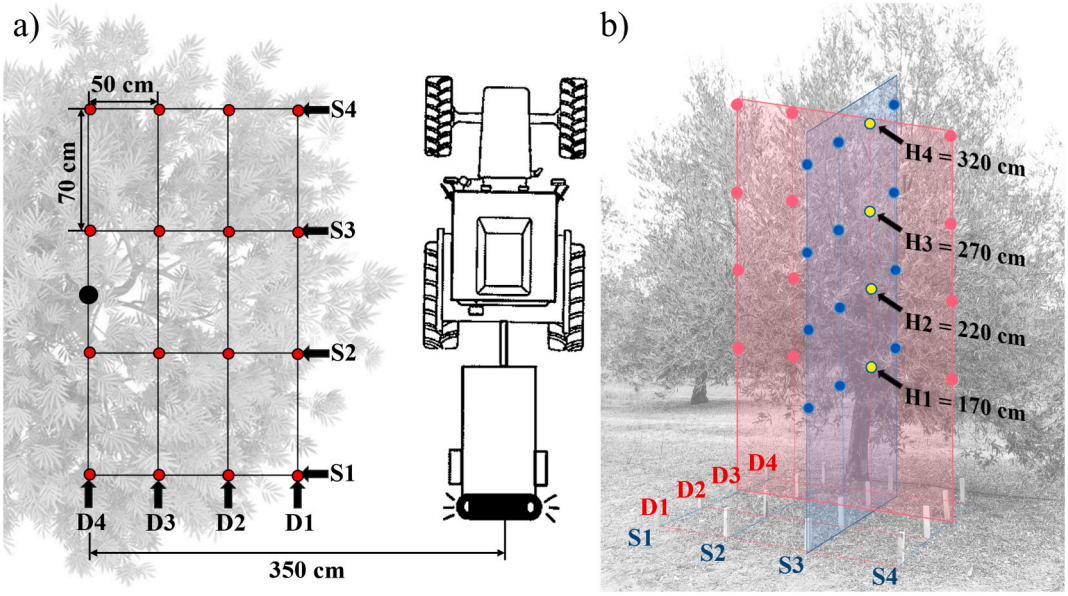

Fig. 2. (a) Distribution of measurement points from top view and (b) example of measurement point distribution for S3 and D3 planes.

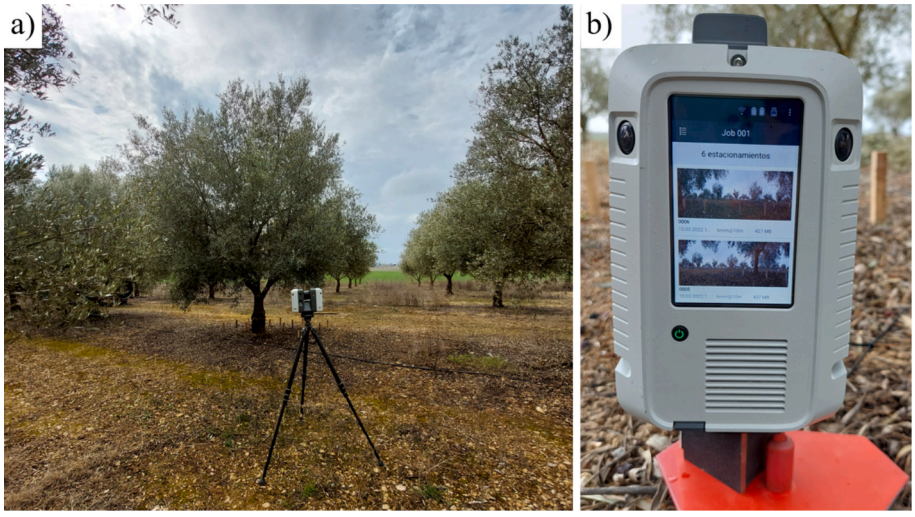

Fig. 3. Vegetation characterization using the LEICA RTC360 laser scanner.

It should be noted that the effective air inlet point location is determined by the local canopy boundary at each section and height, because olive crowns are not perfectly symmetric. Thus, two trees with the same total volume may exhibit very different local perimeters along the measurement line. Moreover, the trials in this study were conducted on one half of each tree. Consequently, the relative distance (D_R) of each predefined depth (D1 – D4) was determined with respect to the air inlet point at the canopy perimeter. To obtain these distances, an individual YZ-plane slice was extracted from the point cloud for each section of the five trees, and the distance between the point cloud contour (canopy perimeter) and D1 was measured on that slice. The remaining depths (D2, D3, D4) were defined at 50 cm cumulative increments from D1.

The number of impacts (NI) was derived from the terrestrial LiDAR point cloud as a quantitative descriptor of vegetation interception. After data acquisition, the cleaned point cloud was discretized using a voxelization approach. Regular voxels of 50 × 50 × 70 cm were defined, matching the dimensions of the experimental sampling grid used for air velocity and spray distribution measurements. For each voxel, NI was computed as the number of LiDAR returns contained within its volume, providing a localized measure of vegetation interception density within the canopy. In this way, 64 voxels were obtained, each containing the corresponding number of points, to subsequently evaluate NI variations within the canopy.

In addition, an accumulated number of impacts (NIa) was computed to account for the cumulative interaction between airflow and vegetation structure along the penetration path. This cumulative formulation was adopted to reduce sensitivity to local point density losses and to provide a more robust descriptor of the overall structural resistance encountered by the airflow within the canopy. NIa was calculated as the cumulative sum of NI values from the canopy outer boundary to each in-canopy measurement point along the airflow direction (Y-axis). Due to the high magnitude and skewed distribution of raw NIa values, a logarithmic transformation was applied prior to subsequent data analyses.

2.2.2. *Manual canopy characterization*

Once trials were finalized, and with the objective of categorizing the olive trees by empirically obtained density parameters, as well as correlating these results with LiDAR measurements, a manual defoliation process was carried out in each experimental tree within small vegetation volumes (8,000 cm^3) at sampling points S2H2 and S3H2 at all

depths, using a hollow cube with dimensions of 20 × 20 × 20 cm. Following the methodology of Miranda-Fuentes et al. (2016), leaf surface area from each cube was determined by weighing the samples and using the previously characterized relationship between the leaf area and weight. Finally, following the hypothesis of previous studies, such as Llorens et al. (2011), which reported good correlations between leaf area index (LAI), determined through destructive methods, and the number of impacts m^{-1} obtained from LiDAR point clouds, the relationship between the number of LiDAR impacts recorded within the volume of defoliated cubes and leaf area density (LAD, m^2 m^{-3}) experimentally determined by defoliation was quantified. For this purpose, R Commander package from R Statistical Software (Version 2.9–5, R Foundation for Statistical Computing, Vienna, Austria) was used.

2.3. Air velocity characterization within the canopy

Air velocity profile (m s^{-1}) inside the canopy was characterized for two airflow configurations associated with the fan gearbox position, which included low and high gearbox settings (configurations C1 and C2, respectively), with airflow rates of 51,193.3 m^3 h^{-1} and 65,467.1 m^3 h^{-1}, respectively. Air velocity map for this equipment was previously studied in laboratory trials, that characterized airflow fan inlet and air velocity behavior around the sprayer (Vigo-Morancho et al., 2024). In this sense, described air velocities at the outlet of the diffusers performed mean ± SD values of 18.56 ± 3.26 m s^{-1} and 22.73 ± 4.29 m s^{-1} for C1 and C2, respectively, on the left side (rear view).

Considering canopy gridding, described in section 2.2, the temporal average of the air velocity generated by the sprayer, which was placed perpendicularly to each section, was registered for both sprayer configurations using a vane probe anemometer (Model 410–1, TESTO, Lenzkirch, Germany). The anemometer recorded data at a frequency of 2 Hz over a 20 s period at each point (measurement range 0.4 to 20 m s^{-1}; resolution 0.1 m s^{-1}) (Fig. 4). The vane anemometer was oriented along the main airflow direction at each sampling point in order to capture the maximum local air velocity. Air velocity at each point was defined as the temporal mean of the 20 s recording period once the probe was aligned with the predominant airflow direction.

In addition to the measurements taken at the 64 grid points, air velocity was measured at sixteen canopy boundary inlet points ($v_{0,}$ m s^{-1}), defined by sections and heights, and compared with air velocity predictions ($v_{P,}$ m s^{-1}) computed using a previously developed laboratory regression model (Vigo-Morancho et al., 2024) that related air velocity to diffuser distance and airflow configuration (R^2 = 0.915). V_P was obtained by using the diffuser to canopy boundary distance, calculated from the relative distances described in subsection 2.2.1.

In order to explain air velocity behavior inside the canopy as a function of the main explanatory parameters, a linear regression model was developed and validated following a leave-one-out cross-validation (LOOCV) procedure. For each iteration, one observation was excluded from the dataset, the model was refitted using the remaining data, and the excluded observation was predicted. Model accuracy was summarized by the cross-validated coefficient of determination (R^2_{cv}) and the root mean squared error (RMSE).

Fig. 4. Air velocity (m s^{-1}) measurement inside the canopy using a vane probe anemometer.

2.4. Spray distribution

The influence of airflow configuration on spray distribution was assessed across the canopy. For this purpose, water sensitive papers (WSP) and filter collectors for coverage and quantitative assessment of product distribution, respectively, were located at all measurement points. Large vertical posts were fixed to the wooden stakes shown in Fig. 4, which defined measurement sections and depths (Fig. 5a). Those posts allowed fixing each artificial collector at its corresponding height (Fig. 5b) for spray distribution assessment.

The sprayer, equipped with D10 DC45 Teejet nozzles, worked at 100% PWM valves duty cycle and 5.0 bar pressure, providing a flow rate of 5.6 L min^{-1}, quantified for each single nozzle following the ISO 5682–2:1997 standard (ISO, 1997). Forward speed, according to traditional farmer's practices, was set at 6.1 km h^{-1}, leading to an application dose of 1,260 L ha^{-1}. WSPs were processed with ImageJ (v1.52a, National Institutes of Health, Bethesda, MD, USA) to quantify percent coverage for each sample. Filter papers were evaluated following the protocol of Garcia-Ramos et al. (2009), using manganese chelate as tracer. Trials were conducted at 1.5 L of tracer per 1,000 L of water, yielding a Mn concentration of 135 mg L^{-1}. During field sampling, filter papers were placed in Falcon tubes for laboratory extraction. Samples were rinsed with a 0.05 N nitric acid solution, and manganese concentrations (mg L^{-1}) were determined by atomic absorption spectrometry (SpectrAA 110, Varian Inc., Palo Alto, Santa Clara, CA, USA). Finally, considering washing volume and filter surface, the amount of Mn in each one (μg cm^{-2}) was calculated.

Meteorological data were recorded in situ to ensure suitable conditions for all trials. Atmospheric wind speed (m s^{-1}) was measured using a vane probe anemometer (0635 9532, TESTO, Lenzkirch, Germany), while relative humidity (%) and temperature (°C) were recorded using a digital thermo-hygrometer (HI 93640, Hanna Instruments, Padova, Italy). Measurements of each parameter were taken both before and after each trial, in accordance with the specific configurations established for each test.

2.5. Data analysis

Air velocity data were analyzed in IBM SPSS Statistics (Version 29, IBM Corp., Armonk, NY, USA) to examine the influence of independent variables, related to canopy characteristics, sprayer airflow configuration and operational parameters (height and depth), on air velocity measured within the canopy. Air velocity normal distribution was verified using the Kolmogorov-Smirnov test and homogeneity of variances among groups was evaluated through Levene's test. The effects of independent variables were examined with univariate tests. When assumptions were met, one-way ANOVA was applied with Tukey's post-hoc comparisons; when homoscedasticity was not met, Tamhane's test was used.

The data distributions associated with canopy coverage and deposition did not meet the normality criteria. Therefore, non-parametric tests, such as the Kruskal–Wallis test, were used to evaluate the effect of the previously defined independent variables on these parameters.

The Spearman's rank correlation test was applied to assess the relationship between these parameters and the air velocity values recorded at the same sampling points.

Fig. 5. Vertical posts located at each plane of measurement (a) and artificial collectors fixed at each height of each post (b). Example for olive 1 (O1).

3. Results and discussion

3.1. Olive tree characteristics

3.1.1. Canopy volume

Fig. 6 shows canopy structure obtained from LiDAR scans of each tree, hereafter defined as O1 to O5, and the reference stakes that define the vertical planes. The largest total volumes corresponded to O4 and O5, with 41.36 m^3 and 45.39 m^3, respectively. An intermediate volume was determined for O1 (32.92 m^3), while the smallest volumes were those of O3 and O2, with 27.72 m^3 and 22.43 m^3, respectively.

Volumes obtained from the present study were consistent with the

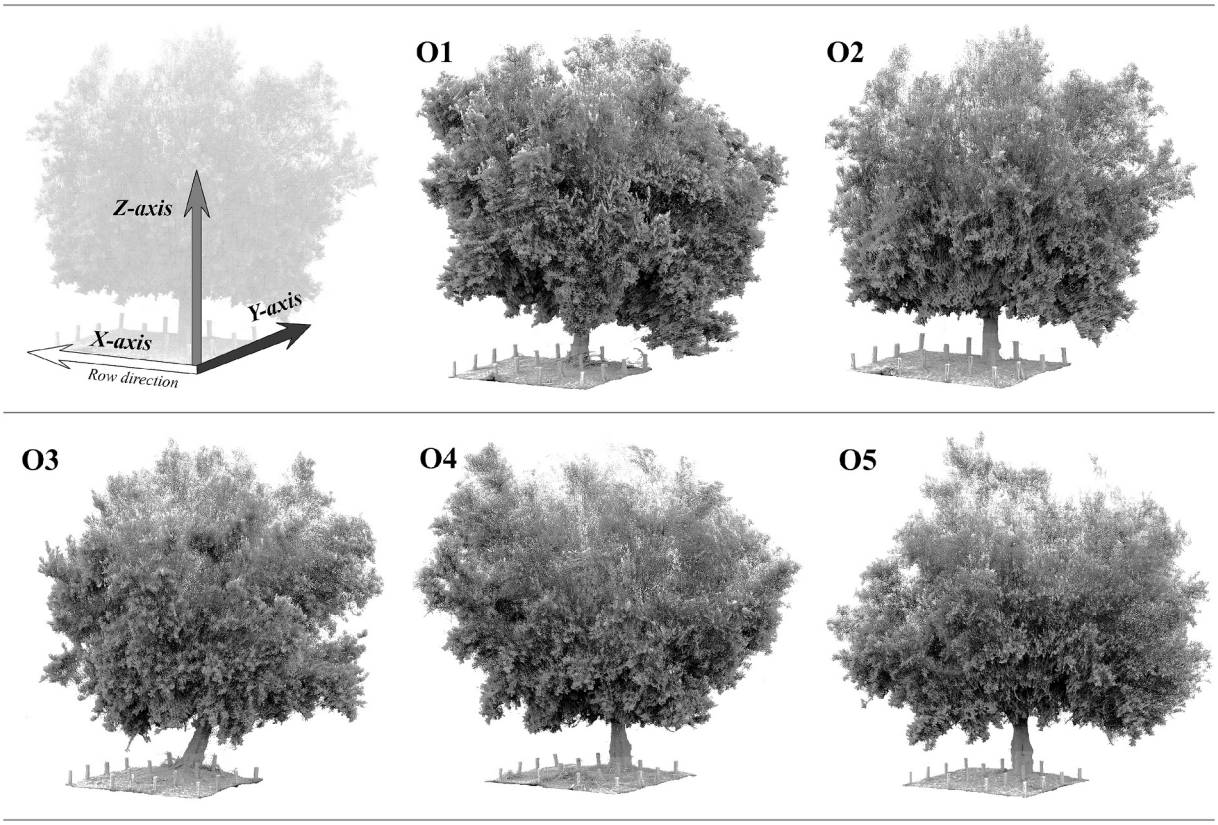

Fig. 6. Canopy structure of each experimental olive tree, from O1 to O5, measured with LiDAR scan. The distance between stakes along the X-axis was 70 cm (planes D1 to D4), and the distance between stakes along the Y-axis (planes S1 to S4) was 50 cm.

model proposed by Miranda-Fuentes et al. (2015), developed for traditional olive trees as a function of the Mean Vector, $\overline{MV}$, computed from the lengths of crown-projection radii within 45° angular intervals. This model proved to be a valuable and practical approach for estimating tree volume, particularly for trees with high canopy symmetry (O2 and O3).

Fig. 7 shows the distribution of the partial volume obtained for each horizontal slice as a function of height above ground for each of the five characterized olive trees. The most voluminous olive trees were also the tallest, exceeding 5 m in height (O4 and O5). In these trees, the maximum perimeter occurred at approximately 3.5 m above ground, whereas in trees O1, O2, and O3 the largest partial volume was recorded at around 2.6 m.

Table 1 reports the relative distance of D1 to the perimeter by section and tree, the standard deviation quantifies the vertical variability within a given section and tree.

3.1.2. Canopy density

Leaf area density (LAD, $m^2\ m^{-3}$), determined by manual defoliation, averaged 3.46, 3.44, 1.93, 2.79 and 2.49 $m^2\ m^{-3}$ for olive trees O1 to O5, respectively. Thus, the densest canopies did not correspond to the most voluminous trees. The relationship between experimentally derived LAD values and the number of LiDAR impacts (NI) within the same sampled volumes (20 x 20 x 20 cm) showed a moderate association, with a coefficient of determination of $R^2 = 0.61$ (Fig. 8a). Notably, the density categorization based on LiDAR impacts showed the same overall pattern as LAD (Fig. 8b), however, it must be considered that LAD do not fully represent the structural elements. Woody components intercepted by the LiDAR beam contribute to the number of impacts but are not captured by defoliation-based measurements, thus, at specific locations, primarily those associated with woody branches presence, the discrepancy between manual measurements and LiDAR scans reduced the correlation between the two variables.

Voxel-based analysis within the sampling grid (4.725 m^3) estimated NI for each 50 × 50 × 70 cm voxel (0.175 m^3), covering depths D1 − D4 at each height and section. NI values showed high spatial variability across voxels, canopy depths ($p = 0.007$), and heights ($p < 0.001$), reflecting the heterogeneous distribution of vegetation elements. When considered individually, local NI values did not exhibit a consistent relationship with in-canopy air velocity. This observation supported the adoption of the accumulated NI (NIa) to represent the progressive interaction between the airflow and the vegetation structure from the canopy boundary toward the interior. NIa, computed for each measurement point, defined the number of impacts between the outer canopy boundary and measurement points along depths. Values are presented on the natural-log scale as heat maps in Fig. 9, shown as a function of depth and height for each tree. NIa increased from D1 to D4 and decreased with height. Among trees, O1 showed the highest NIa, while O3 performed the lowest values across heights and depths.

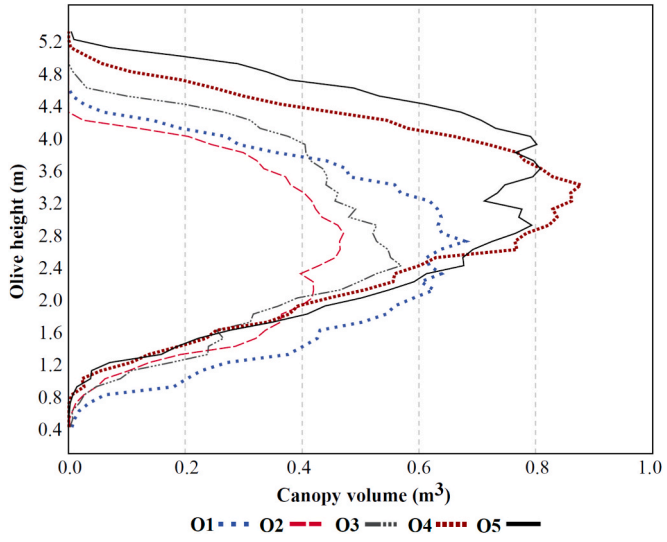

Fig. 7. Volume of each transverse slice versus height above ground for the five studied olive trees (O1 − O5).

Table 1
Mean relative distance (± SD) from D1 to the canopy perimeter for each tree section. O1 – O5 and S1 − S4 indicate olive trees 1–5 and sections 1 - 4. If D1 coincided with the canopy boundary air inlet point, value is shown as (–).

Olive tree	Mean relative distance ± SD (D1- canopy perimeter, cm)			
	S1	S2	S3	S4
O1	–	57.00 ± 37.86	53.50 ± 34.12	46.25 ± 18.40
O2	16.00 ± 10.78	5.50 ± 7.00	18.50 ± 19.97	2.25 ± 3.05
O3	–	8.50 ± 9.09	49.00 ± 33.00	32.75 ± 35.26
O4	55.75 ± 22.70	61.50 ± 29.68	79.00 ± 19.51	90.75 ± 28.24
O5	35.50 ± 37.98	56.00 ± 38.99	71.25 ± 19.08	34.50 ± 50.17

Given the absence of established reference thresholds for NIa, a data-driven approach was adopted to define vegetation density categories. The histogram of log (NIa) frequencies was therefore examined, and the mean value of the normal distribution, log (NIa) = 4.7, was selected as a non-arbitrary threshold representing the central tendency of the data to define two vegetation density classes. Accordingly, low-density (LD) conditions corresponded to log (NIa) < 4.7, whereas high-density (HD) conditions corresponded to log (NIa) ≥ 4.7. The objective of this classification was to use NIa as a structural descriptor to evaluate its influence on in-canopy air velocity behavior. Therefore, the subsequent airflow analysis focuses on the comparison between LD and HD conditions as representative vegetation density scenarios.

3.2. Air velocity and canopy interaction

Airflow characterization within the canopy was conducted on several days in March, under conditions suitable for obtaining reliable air velocity measurements. Across all trials, the mean values of temperature, relative humidity, and atmospheric wind speed were 9.8 °C, 41.3%, and 0.5 m s^{-1}, respectively.

Air velocity at the canopy boundary (v_0) varied according to the equipment configuration, with higher v_0 obtained for C2, regardless of the distance between each boundary inlet point and the sprayer diffusers, which mainly varied through sections. Across the olive trees, the mean v_0 for C2 was 12.42 ± 5.03 m s^{-1}, compared with 9.07 ± 3.82 m s^{-1} for C1. The highest v_0 values were observed in olive trees with larger canopy volumes and, consequently, in canopy boundary points located closer to the diffusers, mainly associated with S2 and S3 (i.e., the central measurement sections) and heights H1 and H2 (170 and 220 cm above ground). At these heights, in addition to being closer to the canopy, they were associated with the diffusers that generated the greatest outlet air velocity, consistent with the previous work by Vigo-Morancho et al. (2024). Specifically, among the six diffusers located on each side of the sprayer, there was a variation in the magnitude of the outlet air velocity, with higher values recorded for the three lower diffusers of the sprayer (21.48 ± 1.09 m s^{-1} vs. 15.65 ± 0.31 m s^{-1} for C1, and 26.19 ± 2.71 m s^{-1} vs. 18.27 ± 3.34 m s^{-1} for C2). This variation in v_0 across heights can therefore be explained by the corresponding variation in the outlet air velocity of the sprayer. Once inside the canopy, the higher air velocity observed for C2 relative to C1 at a given point remained consistent across depths and heights in all olive trees ($p < 0.05$). As shown in Fig. 10, Air velocity entered at D1 and then decreased approximately linearly toward the canopy, with reductions of 4.05 m s^{-1} per depth level ($p < 0.05$).

With increasing height above the ground, air velocity decreased significantly ($p < 0.05$), at an average rate of 0.049 m s^{-1} per cm. Nevertheless, this reduction was not uniform, since factorial ANOVA

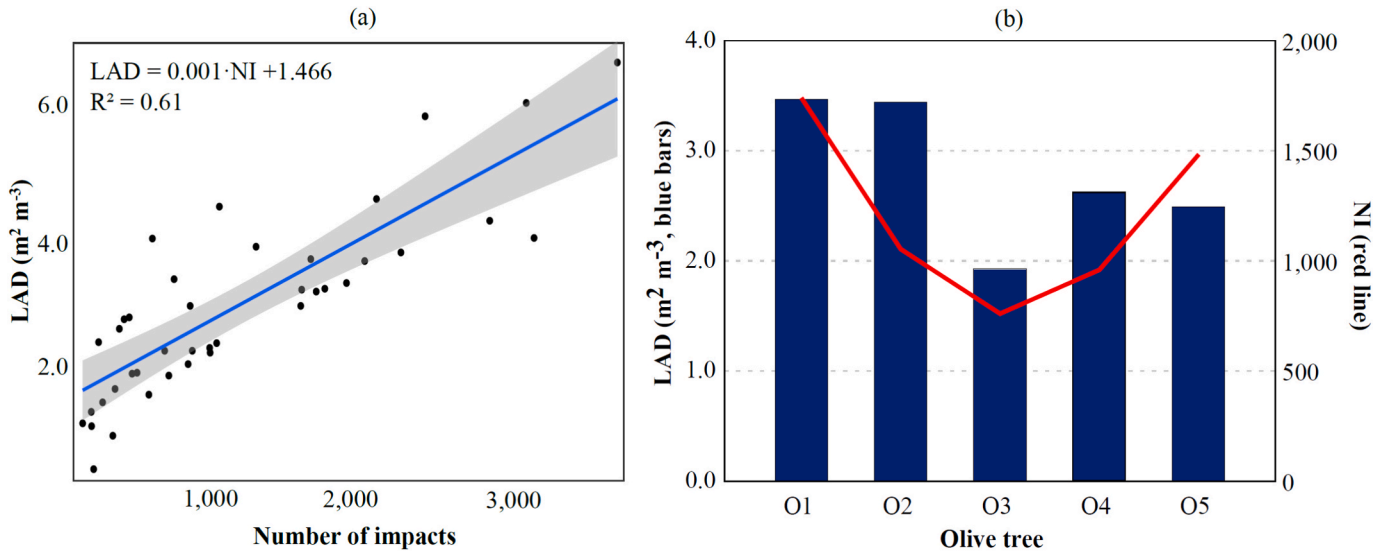

Fig. 8. (a) Relationship between leaf area density (LAD, $m^2\ m^{-3}$) and the number of LiDAR impacts (NI) within the same sampled volumes and (b) mean LAD (blue bars, left y-axis) and NI (red line, right y-axis) for trees O1 to O5.

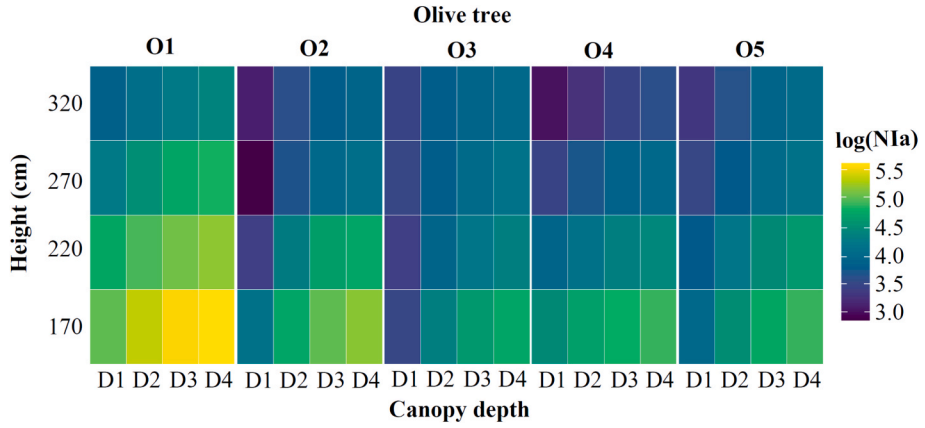

Fig. 9. Heat maps of accumulated LiDAR impacts (NIa) by canopy depth (D1 to D4; D1 = 150 cm from the trunk plane, D4 = at the trunk plane)) and height (170–320 cm) for each olive tree (O1 – O5).

allowed determining an interaction between depth and height (p = 0.047). For the upper heights (270 and 320 cm), the gradient of air velocity decay with depth was lower compared to 170 or 220 cm. These results are consistent with Yan et al. (2024), who also observed air velocity decreasing with increasing heights in vineyards, and with Jeon and Zhu (2024), who documented air velocity decay profiles in apple orchards using sprayers equipped with variable air assist systems.

NIa categorization also had a significant effect on air velocity within the canopy (p = 0.003). Zones classified as high accumulated vegetation density (HD) showed an average reduction of 0.144 m s^{-1}, indicating a greater decrease of air velocity in denser canopies. This effect was consistent across the profile, as it did not interact with sprayer configuration, depth, or height. However, its magnitude was smaller than the other variable, which remained the main factors shaping airflow within the canopy.

In order to provide a practical basis for decision-making regarding pneumatic system adjustment of air assisted sprayers, air velocity within the canopy was modeled as a function of the air velocity at the canopy boundary (v_0, m s^{-1}), which is directly related to sprayer configuration and the distance from diffusers to the canopy, height above the ground (H, cm), the relative distance from the canopy boundary toward the trunk (D_R, cm) and the vegetation density category (DC = 1 for high density; 0 for low density). The fitted regression model is summarized in Eq. (1):

$$v\ (m\ s^{-1}) = I + av_0 + bD_R + cH + d(D_R \cdot H) + eDC \quad (1)$$

Where I is the intercept and a, b, c, d and e, the regression coefficients. The estimated parameters (intercept, coefficients, and model fit) are shown in Table 2. The model explained 71.9% of variance ($R^2 = 0.72$; p < 0.0001).

Basic graphical diagnostics, such as residuals versus fitted and Q – Q plots, were examined to verify residual normality and homoscedasticity. Additionally, overall predictive accuracy, assessed via LOOCV procedure, yielded a cross-validated coefficient of determination $R^2_{cv} = 0.713$ and RMSE = 1.606. Fig. 11 displays observed versus predicted values of air velocity obtained from multiple linear regression model.

Hong et al. (2018) simulated airflow within the canopy and found that increasing canopy depth, tree height, and canopy density systematically decreased air velocities inside the canopy, in agreement with negative coefficients for D_R, H and HD, defined in this study.

The importance of understanding the wind map generated by a hydropneumatic sprayer, and therefore being able to determine the air velocity at the canopy boundary (which influences the air velocity within the crop), is clearly demonstrated by the results obtained in this research (equation (1). This finding could serve as a basis for

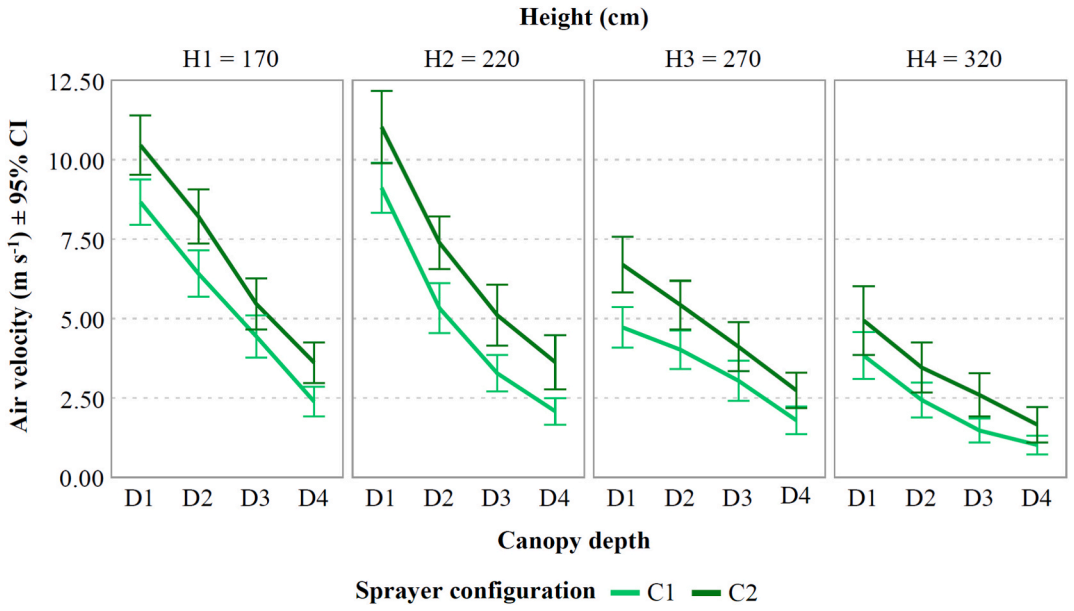

Fig. 10. Mean air velocity (m s^{-1}) ± 95% CI as a function of canopy depth (D1 = 150 cm from trunk plane; D4 = trunk plane), height above the ground (cm) and sprayer configuration (C1 and C2 correspond to low and high gearbox settings, respectively).

Table 2
Regression coefficients for v (m s^{-1}) as a function of canopy boundary air inlet velocity (v_0, m s^{-1}), determined by sprayer configuration and diffuser distance to the canopy perimeter; the relative distance from the canopy boundary (D_R, cm); the height above the ground (H, cm) vegetation density category (DC = 1 for high density; 0 for low density). R^2 = 0.719.

Parameter	Estimate	Standard Error	*p*-value
Intercept	14.561	0.630	< 0.001
v_0	0.213	0.016	< 0.001
D_R	−0.065	0.004	< 0.001
H	−0.035	0.005	< 0.001
D_R·H	$1.5 \cdot 10^{-4}$	$1.7 \cdot 10^{-5}$	< 0.001
DC	−0.790	0.159	< 0.001

encouraging equipment manufacturers to include this information in their catalogs, allowing for objective data-driven adjustments to the system (fan revolutions, vane position, nozzle outlet width).

3.3. Coverage and deposition

The distribution of spray within the olive canopy, evaluated through the percentage of coverage measured on WSP, and the deposition, quantified in the laboratory in terms of tracer concentration, provided further insight into how the factors previously analyzed in relation to air velocity influence spray quality. Across all trials, which were carried out between April and May, the mean values of temperature, relative humidity, and atmospheric wind speed were in this case 25.6 °C, 30.7%, and 1.6 m s^{-1}, respectively.

The overall mean coverage was 44.0%, with minimum values below 5.0% and maximum values approaching 90.0%. Coverage showed marked variability associated with both the application parameters and the structural characteristics of the vegetation. Specifically, a clear effect of canopy depth was observed on the percentage of coverage. Mean values decreased progressively from 63.1% in the outermost zone (D1) to only 24.6% in the innermost zone (D4), revealing a gradual loss of deposition efficiency as the airflow and droplets encountered greater resistance within the foliage.

In addition, canopy height showed a significant influence on coverage ($p < 0.05$). Upper canopy layers received less product, with mean coverage values that decreased from 48.6% at 170 cm to 35.1% at

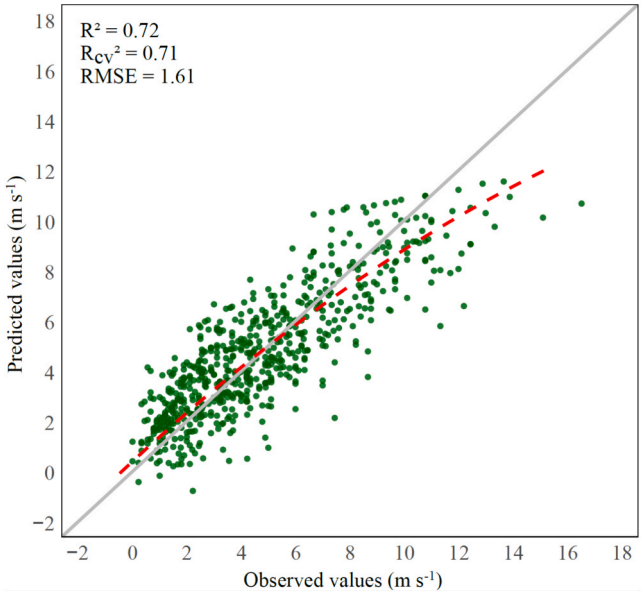

Fig. 11. Observed and predicted air velocity values (m s^{-1}) obtained from regression model. R^2: calibration coefficient of determination; R^2_{cv}: cross-validation coefficient of determination; RMSE: Root Mean Square Error. Grey solid line represents the 1:1 line. Red dashed line represents the best fit for the plotted points.

320 cm, likely due to airflow dispersion and the loss of air velocity magnitude of the ascending airflow. Consistent with the air velocity measurements within the canopy, the reduction in coverage with increasing height was particularly pronounced in the inner canopy layers, where high leaf density and greater distance from the sprayer limited droplet penetration. The spatial pattern of decreasing coverage throughout the canopy, as influenced by height and sprayer configuration, for both vegetation categories, is presented in detail in Fig. 12.

In LD zones, mean coverage reached 48.7%, whereas in HD zones it decreased to 39.1%. Regarding sprayer settings, results showed a slight improvement with C2, yielding an average coverage of 47.1% compared with 41.2% under C1. This improvement was slight at depths D1 and D2,

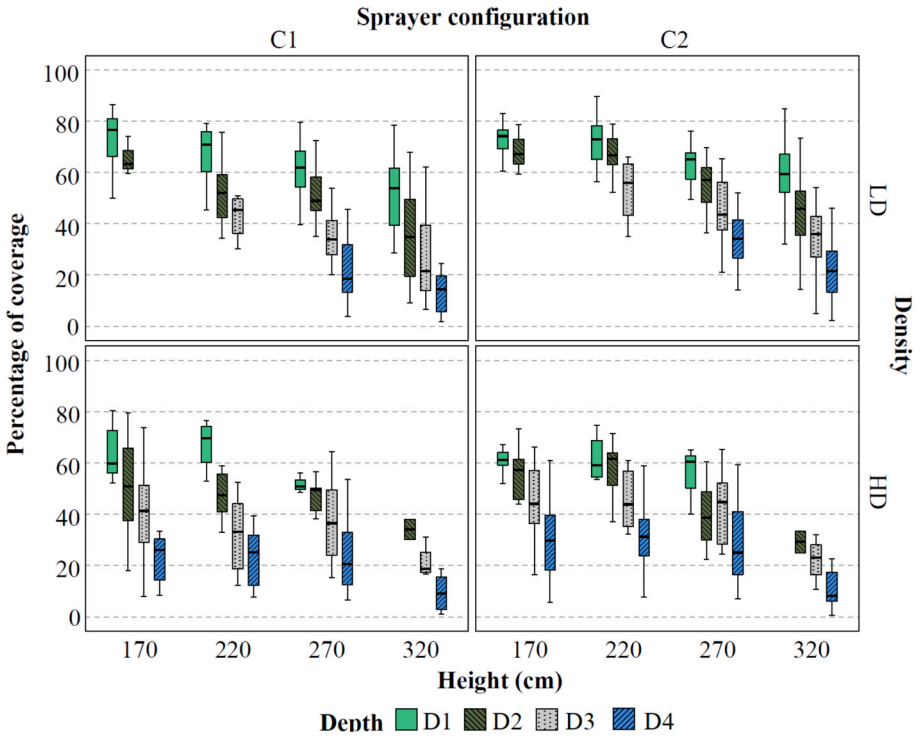

Fig. 12. Percentage of coverage as a function of evaluation height (170–320 cm), canopy depth (D1–D4), canopy density (LD: low; HD: high), and sprayer configuration (C1 and C2). In each group, the central line within the box represents the median, the upper and lower box limits correspond to the interquartile range (IQR, between the 25th and 75th percentiles), and the whiskers indicate the 95% confidence interval.

where, considering each depth together with a given height and canopy density, the Kruskal–Wallis ANOVA showed no significant differences between configurations. However, the improvement observed under C2 was significant compared with C1 in the deeper layers (D3 and D4), where the increase in percentage of coverage was statistically significant in all cases ($p < 0.05$), except at the highest sampling height in D4, for which configuration C2 also exhibited relatively low coverage values (below 20%).

Similar results for deposition analysis within the canopy were observed. In general, the amount of Mn recovered per unit surface area decreased from the canopy exterior toward the interior, following the trend D1 > D2 > D3 > D4 in nearly all evaluated combinations, with global mean deposition values of 1.22, 0.72, 0.39 and 0.23 μg cm^{-2} for D1, D2, D3 and D4, respectively. This pattern was consistent in both LD and HD zones, although the decrease in deposition was more pronounced in HD. In general, an increase in canopy density resulted in lower deposition values across the sampling points, with mean global values of 0.41 μg cm^{-2} compared to 0.84 μg cm^{-2} obtained LD zones, mainly associated with sampling points at greater heights and shallower depths.

Sampling height also conditioned deposition, as height increased from 170 to 320 cm, a progressive decrease in Mn was observed, especially pronounced at the inner depths. Additionally, the sprayer configuration affected spray deposition, C2 tended to yield higher values than C1, with global means of 0.55 vs. 0.73 μg cm^{-2} for C1 and C2, respectively, indicating a superior ability of C2 to transport and disperse

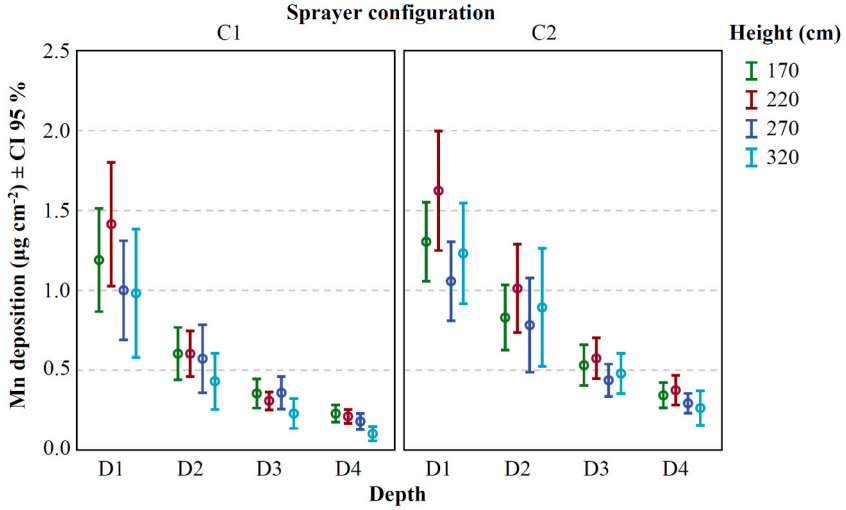

Fig. 13. Manganese (Mn) deposition (μg cm^{-2} ± 95% CI) within the canopy as a function of canopy depth (D1 – D4), sampling height (170–320 cm), and sprayer configuration (C1 and C2).

the spray into the canopy interior. Fig. 13 shows the distribution of Mn deposition within the canopy as a function of sampling height, depth, and sprayer configuration. In both configurations, deposition decreased progressively from the outer (D1) to the inner canopy zones (D4), with higher values generally obtained under C2. The combined effect of height with depth was also evident, as deposition tended to decline toward the upper canopy layers, particularly at the inner depths. Those results align with those obtained by Godoy-Nieto et al. (2022), who observed, both in intensive and traditional olive trees, a sharp decrease in deposition through canopy depths, regardless the sprayer used in their experiments.

In general, coverage and deposition results suggested that configuration C2, associated with greater airflow and higher air velocity within the canopy, led to enhanced spray distribution on the leaf surface. Nevertheless, despite this overall improvement, product penetration remained insufficient in certain zones, particularly in the inner and upper canopy zones, assuming 30% as the minimum threshold for effective treatment, as defined by some authors (Salcedo et al., 2020; Yan et al., 2024).

3.3.1. *Influence of air velocity on spray distribution*

The areas where the lowest coverage and deposition values were obtained coincided with the zones where the lowest air velocities. The Spearman correlation test showed positive and significant associations among the three variables ($n = 640$). Air velocity was strongly correlated with spray coverage ($\rho = 0.744$, $p < 0.001$) and also correlated with Mn deposition ($\rho = 0.690$, $p < 0.001$). In turn, coverage and deposition exhibited the strongest association ($\rho = 0.855$, $p < 0.001$). Overall, these results indicate that higher air velocities are associated with greater coverage and deposition, and that coverage and deposition vary in a closely parallel manner within the canopy. Under the present conditions, coverage may serve as an operational indicator of deposition performance, while the positive relationship with air velocity underscores the importance of optimizing air assistance to maximize droplet penetration and spray performance.

When selecting observations with canopy coverage below 30%, the data were concentrated primarily in trees O1, O4, and O5. Tree O1 was mostly associated with NIa values categorized as HD, whereas O4 and O5 exhibited larger canopy volumes. In these cases, the frequency distribution of air velocity revealed a unimodal grouping, in which 65% of the air velocity values were clustered at magnitudes below 2 m s^{-1}, supporting this value as a practical minimum threshold to secure adequate coverage throughout the canopy under present study conditions. Furthermore, 90% of deposition values associated with air velocities below 2 m s^{-1} were below 0.3 μg cm^{-2}, consistent with Garcia-Ramos et al. (2009), who considered manganese deposition levels of 0.3 μg cm^{-2} indicative of a successful treatment owing to their association with coverage values exceeding 30%.

In a CFD-based analysis by Xu et al. (2022), which was validated with field measurements, air velocities below approximately 2 m s^{-1} were shown to compromise airflow penetration within tree canopies, which is consistent with the findings of the present study. More recently, Feng et al. (2024) evaluated droplet deposition and coverage in apple orchards under different airflow control grades. They observed that when the airflow velocity within the central part of the canopy exceeded 1.5 m s^{-1}, the deposition ratio on both sides of the leaves surpassed 83%, and the coefficient of variation dropped below 33%, indicating an optimal airflow range to ensure efficient and uniform coverage.

The results obtained in this study not only confirm the impact of air assistance on spray applications in three dimensional crops, in this case under a traditional training system, but also demonstrate that the amount of product reaching the innermost canopy zones, and consequently the overall spray quality, varies substantially under identical hydraulic operating conditions when the pneumatic configuration of the sprayer is modified.

From an operational point of view, and based on the predictive models developed in this study, the sprayer could be adjusted so that the selected configuration, according canopy architecture and application settings, ensures an inlet air velocity at the canopy boundary capable of maintaining the minimum air velocity required in the deepest zones of the olive canopy, where adequate coverage levels were observed.

4. Conclusions

This study investigated the interaction between airflow from an air-assisted sprayer and the canopy structure of traditional olive trees by characterizing in-canopy air velocity patterns as a function of vegetation structural parameters, sprayer pneumatic configuration (wind map), and operational settings. integrating LiDAR-based vegetation characterization.

LiDAR-derived metrics proved to be effective predictors of canopy volume and enabled the definition of vegetation density categories. In particular, the accumulated number of impacts (NIa) was validated as a practical structural descriptor for representing canopy density.

Air configuration, canopy depth, height, and density significantly affected the internal air-velocity profile. A multivariate model explained 72% of the observed variability in air velocity, providing a predictive and transferable tool to anticipate airflow behavior from measurable canopy and operational parameters.

Spray coverage and deposition followed the same spatial patterns of air velocity and were strongly correlated with it. Adequate spray performance, defined as coverage $\geq$ 30%, was predominantly associated with local air velocities above 2 m s^{-1}, which in turn resulted in deposition higher than 0.3 μg cm^{-2}.

Therefore, this work provides both experimental and methodological contributions for optimizing airflow adjustment in traditional olive orchards and supports the development of adaptative and more efficient variable-rate air-assisted sprayers.

Finally, this study represents an initial but solid step toward the establishment of a methodological framework for airflow regulation in air-assisted sprayers based on the characterization of the sprayeŕs pneumatic system (wind map) and the LiDAR-derived canopy characterization. The proposed approach was validated under the specific airflow configurations, planting frame, and canopy conditions considered here, and should be interpreted within this experimental context. Further validation under different canopy architectures, airflow settings, and sprayers designs will be required to generalize and consolidate this methodology.

CRediT authorship contribution statement

Alba Vigo-Morancho: Writing – review & editing, Writing – original draft, Visualization, Validation, Software, Resources, Methodology, Investigation, Formal analysis, Data curation. **María Videgain:** Writing – review & editing, Validation, Supervision, Software, Methodology, Investigation, Formal analysis, Data curation. **Alfredo Serreta:** Methodology, Investigation, Data curation. **Antonio Boné:** Supervision, Methodology, Investigation. **Mariano Vidal:** Supervision, Methodology, Investigation, Conceptualization. **Francisco Javier García-Ramos:** Writing – review & editing, Validation, Supervision, Software, Project administration, Methodology, Investigation, Funding acquisition, Formal analysis, Data curation, Conceptualization.

Declaration of competing interest

The authors declare that they have no known competing financial interests or personal relationships that could have appeared to influence the work reported in this paper.

Acknowledgments

This publication is part of the PID2019-104289RB-C43 and

PDC2022-133395-C43 projects, funded by MCIN/ AEI/10.13039/ 501100011033/. The authors would like to express their gratitude to Mañez y Lozano S.L. for providing the sprayer used in this experiment.

Data availability

Data will be made available on request.

References

Badules, J., Vidal, M., Boné, A., Llop, J., Salcedo, R., Gil, E., García-Ramos, F.J., 2018. Comparative study of CFD models of the air flow produced by an air-assisted sprayer adapted to the crop geometry. Comput. Electron. Agric. 149, 166–174. https://doi.org/10.1016/j.compag.2017.09.026.

Biasion, A., Moerwald, T., Walser, B., Walsh, G., 2019. A new approach to the Terrestrial Laser Scanner workflow: the RTC360 solution. *Proceedings of the FIG Working Week*.

Biscamps, J., Garcia-Ruiz, F., Rovira-Mas, F., Gil, E., 2025. Validation of a remote sensor-based spraying strategy in hedge and goblet vineyards. Smart Agric. Technol. 101322. https://doi.org/10.1016/j.atech.2025.101322.

Cross, J., Walklate, P., Murray, R., Richardson, G., 2003. Spray deposits and losses in different sized apple trees from an axial fan orchard sprayer: 3. Effects of air volumetric flow rate. Crop Prot. 22 (2), 381–394. https://doi.org/10.1016/S0261-2194(02)00192-8.

Doruchowski, G., Świechowski, W., Bartosik, A., Hołownicki, R., Godyń, A., 2023. Spray deposition and loss during different application scenarios performed by orchard sprayer with individually adjusted air-jets. *16th Suprofruit workshop* –. Montpellier Sept. 19–21, 2023.

Doruchowski, G., Swiechowski, W., Holownicki, R., Godyn, A., 2009. Environmentally-dependent application system (EDAS) for safer spray application in fruit growing. J. Hortic Sci. Biotech. 84 (6), 107–112. https://doi.org/10.1080/14620316.2009.11512605.

Endalew, A.M., Debaer, C., Rutten, N., Vercammen, J., Delele, M.A., Ramon, H., Nicolaï, B.M., Verboven, P., 2010. A new integrated CFD modelling approach towards air-assisted orchard spraying. Part I. Model development and effect of wind speed and direction on sprayer airflow. Comput. Electron. Agric. 71 (2), 128–136. https://doi.org/10.1016/j.compag.2009.11.005.

Feng, F., Dou, H., Zhai, C., Zhang, Y., Zou, W., Hao, J., 2024. Design and Experiment of Orchard Air-Assisted Sprayer with Airflow Graded Control. Agronomy 15 (1), 95. https://doi.org/10.3390/agronomy15010095.

Fox, R.D., Brazee, R.D., Svensson, S.A., Reichard, D.L., 1992. Air jet velocities from a cross-flow fan sprayer. Transactions of the ASAE 35 (5), 1381–1384. https://doi.org/10.13031/2013.28744.

Fox, R.D., Derksen, R.C., Zhu, H., Brazee, R.D., Svensson, S.A., 2008. A history of air-blast sprayer development and future prospects. Trans. ASABE 51 (2), 405–410. https://doi.org/10.13031/2013.24375.

Garcera, C., Fonte, A., Molto, E., Chueca, P., 2017. Sustainable use of Pesticide applications in Citrus: a support Tool for volume Rate Adjustment. Int. J. Environ. Res. Public Health 14 (7). https://doi.org/10.3390/ijerph14070715.

Garcera, C., Moltó, E., Izquierdo, H., Balsari, P., Marucco, P., Grella, M., Gioelli, F., Chueca, P., 2022. Effect of the Airblast Settings on the Vertical Spray Profile: Implementation on an On-Line Decision Aid for Citrus Treatments. Agronomy 12 (6). https://doi.org/10.3390/agronomy12061462.

Garcia-Ramos, F.J., Vidal, M., Bone, A., 2009. Field evaluation of an air-assisted sprayer equipped with two reversed rotation fans. Appl. Eng. Agric. 25 (4), 481–494. https://doi.org/10.13031/2013.27461.

García-Ramos, F.J., Vidal, M., Boné, A., Malón, H., Aguirre, J., 2012. Analysis of the air flow generated by an air-assisted sprayer equipped with two axial fans using a 3D sonic anemometer. Sensors 12 (6), 7598–7613. https://doi.org/10.3390/s120607598.

Godoy-Nieto, A., Miranda-Fuentes, A., Grella, M., Blanco-Roldán, G.L., Rodríguez-Lizana, A., Gil-Ribes, J.A., 2022. Assessment of spray deposit and loss in traditional and intensive olive orchards with conventional and crop-adapted sprayers. Agronomy 12 (8), 1764. https://doi.org/10.3390/agronomy12081764.

Grella, M., Gioelli, F., Marucco, P., Mozzanini, E., Caffini, A., Nuyttens, D., Zwertvaegher, I., Fountas, S., Athanasakos, L. and Mylonas, N. (2022a). Exploring variable air flow rate as a function of leaf area index for optimal spray deposition in trellised vineyards. *Aspects of Applied Biology: International Advances in Pesticide Application*, 251-260.

Grella, M., Marucco, P., Gioelli, F., Balsari, P., Athanasakos, L., Mylonas, N., Fountas, S., Zwertvaegher, I., Nuyttens, D. and Caffini, A. (2022b). Airblast sprayer electrification for real-time, continuous fan-airflow adjustment according to canopy density during pesticide application in 3D crops. *In VDI-Berichte: LAND.TECHNIK 2022 - The Forum for Agricultural Engineering Innovations* (Vol. 2395, pp. 389-395). VDI Wissenforum.

Gu, C., Zhao, C., Zou, W., Yang, S., Dou, H., Zhai, C., 2022. Innovative leaf area detection models for orchard tree thick canopy based on LiDAR point cloud data. Agriculture 12 (8), 1241. https://doi.org/10.3390/agriculture12081241.

Hołownicki, R., Doruchowski, G., Świechowski, W., Godyń, A., Konopacki, P.J., 2017. Variable air assistance system for orchard sprayers; concept, design and preliminary testing. Biosyst. Eng. 163, 134–149.

Hong, S.-W., Zhao, L., Zhu, H., 2018. CFD simulation of airflow inside tree canopies discharged from air-assisted sprayers. Comput. Electron. Agric. 149, 121–132. https://doi.org/10.1016/j.compag.2017.07.011.

ISO, 1997. Equipment for Crop Protection - Spraying Equipment - Part 2: Test Methods for Hydraulic Sprayers. ISO 5682-2:1997. *International Organization for Standardization Publications, Geneva*.

Jeon, H., Zhu, H., 2024. Development of an Electric Variable Air Assist System for Apple Orchard Sprayers. Journal of the ASABE. https://doi.org/10.13031/ja.15853.

Li, S., Dai, L., Wang, H., Wang, Y., He, Z., Lin, S., 2017. Estimating leaf area density of individual trees using the point cloud segmentation of terrestrial LiDAR data and a voxel-based model. Remote Sens. (Basel) 9 (11), 1202. https://doi.org/10.3390/rs9111202.

Llorens, J., Gil, E., Llop, J., Escolà, A., 2011. Ultrasonic and LIDAR sensors for electronic canopy characterization in vineyards: advances to improve pesticide application methods. Sensors 11 (2), 2177–2194. https://doi.org/10.3390/s110202177.

MAPA, Ministerio de Agricultura, Pesca y Meido Ambiente, 2024a. Encuesta sobre Superficies y Rendimientos (ESYRCE). *Análisis de las plantaciones de olivar en España*. Retrieved from: https://www.mapa.gob.es/dam/mapa/contenido/estadisticas/temas/estadisticas-agrarias/2.agricultura/1.-encuesta-sobre-superficies-y-rendimientos-de-cultivos–esyrce/informes-sectoriales/olivar2024.pdf.

MAPA, Ministerio de Agricultura, Pesca y Meido Ambiente, 2024b. *Inscripción de maquinaria agrícola 2024*. Retrieved from: https://www.mapa.gob.es/dam/mapa/contenido/agricultura/temas/medios-de-produccion/maquinaria-agricola/estadisticas/informe2024.pdf.

Miranda-Fuentes, A., Llorens, J., Gamarra-Diezma, J., Gil-Ribes, J., Gil, E., 2015. Towards an optimized method of olive tree crown volume measurement. Sensors 15 (2), 3671–3687. https://doi.org/10.3390/s150203671.

Miranda-Fuentes, A., Llorens, J., Rodríguez-Lizana, A., Cuenca, A., Gil, E., Blanco-Roldán, G., Gil-Ribes, J., 2016. Assessing the optimal liquid volume to be sprayed on isolated olive trees according to their canopy volumes. Sci. Total Environ. 568, 296–305. https://doi.org/10.1016/j.scitotenv.2016.06.013.

Ortí, E., Cuenca, A., Pérez, M., Torregrosa, A., Ortiz, C., Rovira-Más, F., 2022. Preliminary evaluation of a blast sprayer controlled by pulse-width-modulated nozzles. Sensors 22 (13), 4924. https://doi.org/10.3390/s22134924.

Pagliai, A., Ammoniaci, M., Sarri, D., Lisci, R., Perria, R., Vieri, M., D'Arcangelo, M.E.M., Storchi, P., Kartsiotis, S.-P., 2022. Comparison of aerial and ground 3D point clouds for canopy size assessment in precision viticulture. Remote Sens. (Basel) 14 (5), 1145. https://doi.org/10.3390/rs14051145.

Petrović, I., Sečnik, M., Hočevar, M., Berk, P., 2022. Vine canopy reconstruction and assessment with terrestrial lidar and aerial imaging. Remote Sens. (Basel) 14 (22), 5894. https://doi.org/10.3390/rs14225894.

Reichard, D., Fox, R., Brazee, R., Hall, F., 1979. Air velocities delivered by orchard air sprayers. Transactions of the ASAE 22 (1), 69–0074. https://doi.org/10.13031/2013.34968.

Rovira-Más, F., Saiz-Rubio, V., Cuenca, A., Ortiz, C., Teruel, M.P., Ortí, E., 2024. Open-Format prescription maps for variable rate spraying in orchard farming. Journal of the ASABE 67 (2), 243–257. https://doi.org/10.13031/ja.15750.

Salas, B., Salcedo, R., Garcia-Ruiz, F., Gil, E., 2025. Field validation of a variable rate application sprayer equipped with ultrasonic sensors in apple tree plantations. Precis. Agric. 26 (1), 22. https://doi.org/10.1007/s11119-024-10201-5.

Salas, B., Salcedo, R., Ortega, P., Grella, M., Gil, E., 2022. Use of ultrasound anemometers to study the influence of air currents generated by a sprayer with an electronic control airflow system on foliar coverage. effect of droplet size. Comput. Electron. Agric. 202. https://doi.org/10.1016/j.compag.2022.107381.

Salcedo, R., Fonte, A., Grella, M., Garcerá, C., Chueca, P., 2021. Blade pitch and air-outlet width effects on the airflow generated by an airblast sprayer with wireless remote-controlled axial fan. Comput. Electron. Agric. 190, 106428. https://doi.org/10.1016/j.compag.2021.106428.

Salcedo, R., Pons, P., Llop, J., Zaragoza, T., Campos, J., Ortega, P., Gallart, M., Gil, E., 2019. Dynamic evaluation of airflow stream generated by a reverse system of an axial fan sprayer using 3D-ultrasonic anemometers. effect of canopy structure. Comput. Electron. Agric. 163, 104851. https://doi.org/10.1016/j.compag.2019.06.006.

Salcedo, R., Zhu, H., Zhang, Z., Wei, Z., Chen, L., Ozkan, E., Falchieri, D., 2020. Foliar deposition and coverage on young apple trees with PWM-controlled spray systems. Comput. Electron. Agric. 178, 105794. https://doi.org/10.1016/j.compag.2020.105794.

Sozzi, A., 2011. Estudio del efecto de diferentes caudales de aire sobre la distribución, recubrimiento y cantidad de producto depositado con pulverizador hidroneumático en cítricos (Doctoral dissertation, Universitat Politècnica de València).

Svensson, S.A., 2001. Converging air jets in orchard spraying. Acta Universitatis Agriculturae Sueciae, Agraria, p. 279.

Torrent, X., Llorens, J., Arnó, J., Martínez-Casasnovas, J., Plata, J., Sandonís-Pozo, L., Hajjaj, O. and Escolà, A. (2025). Evaluating NDVI as a proxy for LiDAR-based canopy characterisation in large almond orchards. In *Precision agriculture'25* (pp. 737-744): Wageningen Academic. https://doi.org/10.1163/9789004725232_097.

Vigo-Morancho, A., Videgain, M., Boné, A., Vidal, M., García-Ramos, F.J., 2024. Static and dynamic study of the airflow behavior generated by two air assisted sprayers commonly used in 3D crops. Comput. Electron. Agric. 216, 108535. https://doi.org/10.1016/j.compag.2023.108535.

Xu, T., Zhou, H., Lv, X., Lei, X., Tao, S., 2022. Study of the distribution characteristics of the airflow field in tree canopies based on the CFD model. Agronomy 12 (12), 3072. https://doi.org/10.3390/agronomy12123072.

Xu, W., Su, Z., Feng, Z., Xu, H., Jiao, Y., Yan, F., 2013. Comparison of conventional measurement and LiDAR-based measurement for crown structures. Comput. Electron. Agric. 98, 242–251. https://doi.org/10.1016/j.compag.2013.08.015.

Yan, C., Xu, L., Ma, S., Tan, H., Shen, C., Ma, J., Zhou, H., 2024. Enhancing spray deposition in grape canopies through the development of new prototype air-

disturbance sprayers. Biosyst. Eng. 244, 1–15. https://doi.org/10.1016/j.biosystemseng.2024.05.013.

Zhang, J., Chen, Q., Zhou, H., Zhang, C., Jiang, X., Lv, X., 2024. CFD analysis and RSM-based design optimization of axial air-assisted sprayer deflectors for orchards. Crop Prot. 184, 106794. https://doi.org/10.1016/j.cropro.2024.106794.

Zhou, H., Zhang, J., Ge, L., Yu, X., Wang, Y., Zhang, C., 2021. Research on volume prediction of single tree canopy based on three-dimensional (3D) LiDAR and clustering segmentation. Int. J. Remote Sens. 42 (2), 738–755. https://doi.org/10.1080/01431161.2020.1811917.